A Feasibility Design of PEMFC Parallel Operation for a Fuel Cell Generation System

Hyun-Soo Kang*, Gyu-Yeong Choe*, Byoung-Kuk Lee† and Jin Hur**

Abstract – In this paper, the parallel operation for a FC generation system is introduced and designed in order to increase the capacity for the distributed generation of a proton exchange membrane fuel cell (PEMFC) system. The equipment is the type that is used by parallel operated PEMFC generation systems which have two PEMFC systems, two dc/dc boost converters with shared dc link, and a grid-connected dc/ac inverter for embedded generation. The system requirement for the purpose of parallel operated generation using PEMFC system is also described. Aspects related to the mechanical (MBOP) and electrical (EBOP) component, size, and system complexity of the distributed generation system, it is explained in order to design an optimal distributed generation system using PEMFC. The optimal controller design for the parallel operation of the converter is suggested and informative simulations and experimental results are provided.

Keywords: Current-fed dc/dc Converter, dc/ac pwm Inverter, Parallel Operation, Power Conditioning System, Proton Exchange Membrane Fuel Cell (PEMFC), Voltage-fed dc/dc Converter

1. Introduction

The basic principal operation of fuel cells is a very simple procedure using the recombination of hydrogen and oxygen. As a result, an electric current is produced. Therefore, the fuel cell is an electrochemical device that converts chemical energy directly into electrical and thermal energies. With these features, it could well become a crucial component of future energy with zero-emission. Consequently, during the past several years there have been great improvements in fuel cell technologies due to the major concern to reduce acid gas emissions, CO_2, for pollution free surroundings. In order to understand the basic concept of operating the fuel cell system and the system configuration, the system diagram is shown in Fig. 1.

The most important part of a distinguished fuel cell type is usually the electrolyte, which is used in the fuel cell stack. The proton exchange membrane fuel cell (PEMFC) has a solid polymer electrolyte in which the mobile proton exists. These cells have attractive advantages such as very low-temperature operation and simple structure, but the cost of sophisticated catalysts, electrodes, and the supply of pure hydrogen are definite disadvantages. Instead of using pure hydrogen, it is supplied by way of the methanol as a fuel, and such cells are known as direct methanol fuel cells (DMFC). It has gained its region only in mobile and portable electronics, due to their inherently low powers. Alkaline fuel cells (AFC) have been used on space ships, but despite their reliability, they are slow to react, high in pressure, have an operating temperature above 100℃~200℃, and are easily poisoned by carbon dioxide (CO_2). Phosphoric acid fuel cells (PAFC) were the first commercialized fuel cell product, and they are still used and installed in many parts of the world due to their simple structure, high reliability, and fairly high temperature (~220℃). The solid oxide fuel cell (SOFC) and molten carbonate fuel cell (MCFC) have the interesting features of high operating temperature and are also cheap catalysts. Because of their stack simplicity and ease to increase their capacity, they are usually adopted in distributed generation systems [1]. Also, the basic information of several fuel cell types is presented in Table 1.

In regards to these many types of fuel cells, PEMFC clearly has greater merits when it comes to operating temperature (@80℃) and uncomplicated structure, despite its expensive platinum catalysts. Especially in locomotives and other forms of transportation, the use of PEMFC is a current trend of fuel cell system configuration. Also, for the effort of reducing the catalysts cost and replacing the platinum catalyst with other material, like Pt alloy or non PM, the Pt loading has been researched by many scientists. According to DOE/Freedom CAR targets, the stack cost of 65\$kWe^{-1} in 2005 will be reduced to around 15\$kWe^{-1} in 2015. Therefore, the system cost will be reduced from 125\$kWe^{-1} in 2005 to 30\$kWe^{-1} in 2015 [2].

† Corresponding Author: School of Information and Communication Engineering, Sungkyunkwan Univ., Korea. (bkleeskku@skku.edu)
* School of Information and Communication Engineering, Sungkyunkwan University, Korea.
** School of Electrical Engineering, University of Ulasn, Korea. (jinhur@ulsan.ac.kr)
Received 29 February, 2008 ; Accepted 28 May, 2008

As a result, recent development in fuel cell technology has made the PEMFC system more promising for stationary and transportation application areas up to 200kW [3]. They have the distinctions in high efficiency, high power density, zero-emission and high reliability, as well as high durability in normal operating temperature. In this progress, cost of the catalysts is not only the main issue in the PEMFC system, but the capacity extension of the PEMFC is the significant issue for high power system configurations. Therefore, the parallel operation of the PEMFC is necessary to the high power system, like locomotives or stationary plants.

A practical PEMFC system consists of fuel cell stacks, a fuel supply, an air supply, water, heat treatment sub-systems, and power conditioning systems (PCS). The PCS play the important role of generating and delivering their power from the fuel cell to the loads. By use of this PCS, it becomes a so-called distributed generation system. Therefore the PCS should be operated at high efficiency, high performance, high reliability, and high durability with low cost. Usually this kind of PCS consists of a dc/dc converter and a dc/ac inverter due to the inherent low voltage and high current characteristics of the fuel cell system. Consequently, it is crucial to design this PCS with high efficiency and high reliability, because the reliability of the whole fuel cell system depends on the reliability of the PCS. Until now, many researches have been focused on the operation of the dc/dc converter of the PCS itself and the higher efficiency of the PCS operation [4~10].

The purpose of this paper is the feasibility design and operation of the PEMFC system with shared load and current, which is suitable for the PEMFC parallel operation. As the number of the parallel operation sources increase, the control issue and the active power sharing between the parallel operation systems become more complex and even more complicated. This paper first provides a brief description of the PEMFC structure and its operating

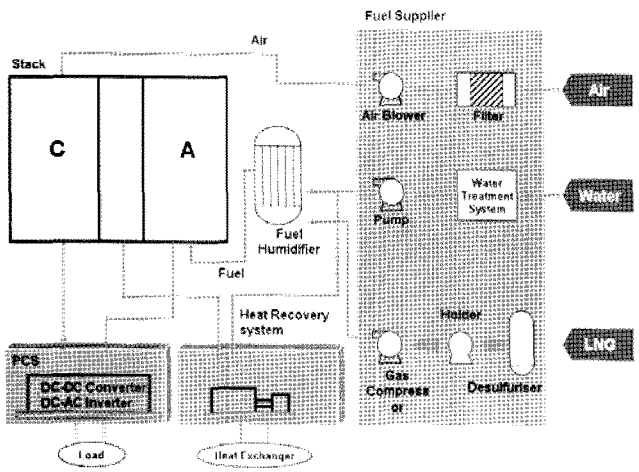

Fig. 1. Fuel cell system diagram

Table 1. The characteristics of diffent types of fuel cells

Fuel Cell Type	Operating Temperature	Electrical Efficiency	Applications
AFC	90 ~ 100°C	60%	Space Shuttle
PEMFC	50 ~ 100°C	53~58% (Vehicles) 25~35% (Stationary)	Vehicles, Lower CHP
DMFC	20 ~ 90°C	Same as PEMFC	Portable electronics
PAFC	150 ~ 220°C	32 ~ 38%	~ 200kW CHP
MCFC	600 ~ 700°C	45 ~ 47%	CHP up to MW
SOFC	650 ~ 1000°C	35 ~ 43%	CHP up to multi-MW

principals. The PEMFC is mathematically modeled with the Nernst equation, three polarizations, fuel crossover /internal current, exchange current, and limit current. Consequently, it is more helpful to understand the function of MBOP and EBOP of the PEMFC. Furthermore, the basic operation of MBOP and EBOP is discussed as they are crucial components of the PEMFC system. Finally, for the feasibility design of a PEMFC parallel operation, two dc/dc converters are designed and a single grid-connected inverter with unity power factor is connected with shared dc link. Informative simulations and experimental results are provided along with the small signal analysis and controller design process.

2. Physical Structure and Operating Principle of a Proton Exchange Membrane Fuel Cell

It is necessary to understand the physical structure and operating principle of the PEMFC for the understanding of the PEMFC system operation. Fig. 2 shows the physical cell structure of the PEMFC. There is an electrolyte membrane in the center. The anode and cathode are located within both sides of the membrane, known as the Membrane Electrolyte Assembly (MEA). The cell MEA consists of anode catalysts, cathode catalysts, and the membrane. The anode and cathode catalysts are applied to the electrolyte membrane using either a rolling, spraying, or inking method. Once the catalysts are fixed to the membrane, the gas diffusion layers (GDL) are deposited onto the MEA, where the perfluorosulfonic acid (PFSA) electrolyte membrane Nafion, is generally used [4]. The gas diffusion layer (GDL) for similarly supporting the fuel exists within both sides of the electrode. The hydrogen ions (H^+) can pass through it. The electrode, catalyst, and carbon are mixed for maximizing the response areas.

A gasket is inserted for sealing up the fuel and is composed of rubber. A bipolar plate is used in the channel as a supporting reactant, water remover, and electron collector. The reactant moves in the channel of the bipolar plate and is removed. The channel plays an important role in fuel cell performance.

There must be a humidified polymer electrolyte because

the proton conductivity is directly proportional to the water content when the hydrogen ion is H_3O^+ [1]. The reaction at the anode is oxidation. The MEA separates two gases, which is the hydrogen ion and the electron. The hydrogen ions move through the membrane to the cathode. The electrons travel the bipolar plate and depart the external circuit creating a useful current. The reaction at the cathode is de-oxidation. The hydrogen ions combine with oxygen to produce water and heat energy. Equations (1) to (3) are the reaction equations at the anode and cathode.

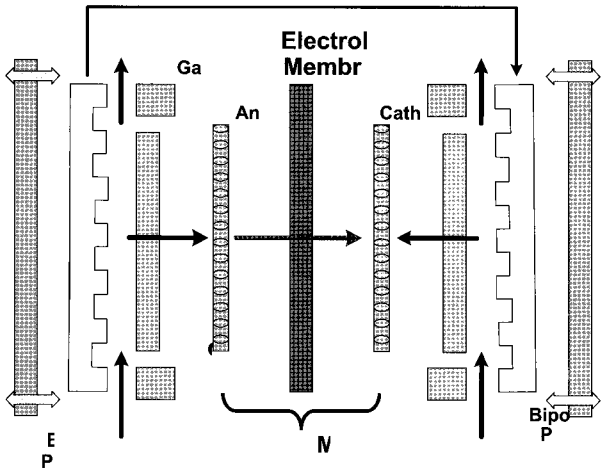

Fig. 2. Physical structure of PEMFC.

$$Anode \quad : H_2 \rightarrow 2H^+ + 2e^- \quad (oxidation) \tag{1}$$

$$Cathode : \frac{1}{2}O_2 + 2H^+ + 2e^- \rightarrow H_2O \quad (deoxidation) \tag{2}$$

$$Overall \quad : H_2 + \frac{1}{2}O_2 \Rightarrow H_2O + Heat \tag{3}$$

3. PEMFC Modeling [5]

3.1 Nernst Model

The chemical energy deciding the fuel cell output is explained by Gibbs free energy. If the reaction of the reactant is reversible, the OCV is 1.229V. However, the real fuel cell output is lower than OCV and it is an important factor of the PEMFC modeling. The Nernst equation can calculate the theoretical voltage at the irreversibility. The electrochemical reaction is then derived in the fuel cell. Equation (4) depicts the Nernst Equation

$$E = E^0 + \frac{RT}{2F}\ln\frac{P_{H_2}P_{O_2}^{\frac{1}{2}}}{P_{H_2O}} \tag{4}$$

where, E^0 is reversible cell voltage, R is gas constant (8.3144 J/mol K), T is temperature in Kelvin scale (K), F is Faraday's constant (96,495 C/mol), and P is partial pressure.

3.2 Three Polarizations

The output voltage of the fuel cell is always lower than OCV due to irreversible losses which are brought on by the polarization. The polarization consists of three parts.

The first, activation polarization, is caused by slowness of the reactions taking place in the surface of the electrodes. Namely, it is generated in case that the reaction of the hydrogen or oxygen is sluggish in the electrolyte. The activation polarization can show the generalized Tafel equation. It is caused by the biggest voltage loss among polarizations of the PEMFC. Equation (5) shows the Tafel equation

$$\eta_{act} = \frac{RT}{\alpha nF}\ln\frac{i}{i_o} \tag{5}$$

where, α is transfer coefficient, n is number of electrons per reacting ion or molecule, i_o is exchange current density, and i is current density.

In order to reduce the activation polarization, one uses the porous electrode and raises the activity coefficient using a catalyst and increases the exchange current density.

The second, ohmic polarization, consists of the electrode resistance, electrolyte resistance, line resistance, and contact resistance of the connector. It can be represented by voltage loss at the resistance. The ohmic polarization has a regular slope and is the actual operating area of the PEMFC. The rating voltage of the ohmic region is 0.6V~0.8V generally. Equation (6) depicts the ohmic polarization.

$$\eta_{ohmic} = IR_T \tag{6}$$

where, $R_T = r_i + r_e + r_c$, r_i is ionic resistance, r_e is electronic resistance, and r_c is contact resistance.

The third, the concentration or mass transport polarization, is caused by changing the concentration of the reactant at the surface of the electrode. In other words, it can be understood by voltage loss caused by shapely discharging the capacitor during the overload from an electrical point of view. This region generates the shape voltage loss and isn't used in actuality. Equation (7) shows the concentration or mass transport polarization

$$\eta_{conc} = \frac{RT}{nF}\ln\left(1 - \frac{i}{i_L}\right) \tag{7}$$

The additional loss is caused by the fuel crossover /

internal current in which the fuel directly passes through the electrolyte without separating the electron and hydrogen ions. The current flows internally without getting out to the external circuit. This is the leakage current from an electrical point of view. The internal current can be represented by (8).

$$i_{int} = e^{\frac{1.04-V}{0.06}} - i \tag{8}$$

3.3 Exchange Current Density and Limiting Current Density

Without the load, in any other condition when the current density is zero, the reaction at the electrode doesn't work. However, the electrode reaction of the fuel cell is actually reacted. Because the ratio of reaction and reverse reaction is equal to each other, it appears as no reaction in the fuel cell [1]. The reaction and reverse reaction is revealed in Equation (9).

$$O_2 + 4e^- + 4H^+ \leftrightarrow 2H_2O \tag{9}$$

The exchange current has the continuous reaction with reverse reaction current at the electrode and electrolyte. The exchange current density is proportional to the catalyst, catalyst area, electrode area, partial pressure of the reactant, temperature, and activity energy. Also, if the exchange current is increased, the activation polarization is reduced. Therefore, it is one of the important factors of efficiency of the fuel cell. The exchange current density can be expressed by Equation (10).

$$I_o = I_o^{ref} a_c L_c \left(\frac{P_r}{P_r^{ref}}\right)^{\gamma} \exp\left[-\frac{E_c}{RT}\left(1-\frac{T}{T_{ref}}\right)\right] \tag{10}$$

where, I_o^{ref} is reference exchange current density at reference temperature, P_r is pressure based on actual catalyst surface area, a_c is catalyst specific area (cm^2/mg), L_c is catalyst loading (mg/cm^2), and γ is reaction order with respect to the reactant.

The limit current density can be derived by use of the relation to ideal gas equation and Fick's law. Equation (11) can be presented by the limit current density.

$$i_L = \frac{nFDP}{RT\delta} \tag{11}$$

where, D is diffusion constant, and δ is thickness of the diffusion layer.

3.4 Fuel Cell Stack Voltage

The operating voltage of the PEMFC stack is equal to the value of OCV minus three polarizations. As well, the pressure proportional to the mass flow exchange rate should be considered at seeking the output characteristic of the fuel cell. The pressure affects the activation and concentration polarization and V-I curve. This can be shown as in Equation (12), the operating voltage of the PEMFC.

$$V_{cell} = E - (i+i_n)r - A\ln\left(\frac{i+i_n}{I_o^{ref} a_c L_c \left(\frac{P_r}{P_r^{ref}}\right)^{\gamma} \exp\left[\frac{E_c}{RT}\left(1-\frac{T}{T_{ref}}\right)\right]}\right) + B\ln\left(1-\frac{i+i_n}{i_L * P}\right) \tag{12}$$

where, Tafel slope , $A = \frac{RT}{\alpha nF}$, $B = \frac{RT}{nF}$

In Fig. 3, the V-I characteristics of the PEMFC by use of the equation that is introduced in this section are revealed. It indicates the OCV and three polarization regions of fuel cell output voltage. Designing the PCS, the operating point of the PCS should be the ohmic polarization region in order to guarantee the safe operation and high efficiency of the system. Usually for the design of a PCS, the power capacity of the fuel cell stack could be calculated as follows, assuming the single cell operating voltage in the ohmic polarization region is 0.7 ~ 0.8V, and the number of cells for the stack is 35, current density of the cell is 600mA/cm^2, and the area is 80cm^2. The fuel cell stack output voltage is 24.5 ~ 28V, the output current is 48A, and the output stack power is 1176 ~ 1344W.

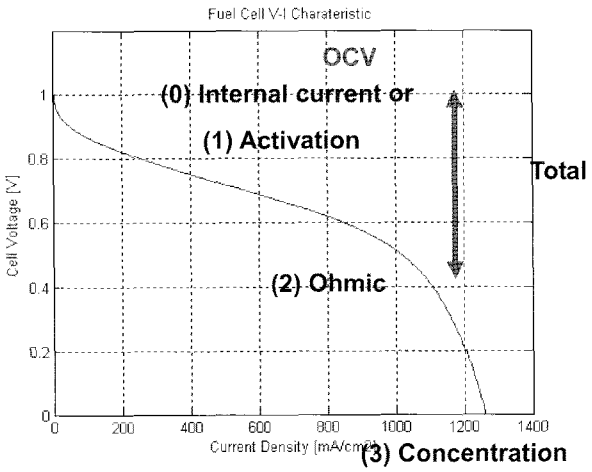

Fig. 3. The V-I characteristics of a fuel cell.

Also similar to batteries, it is easy to make the single fuel cell stack module deploy parallel connection because serial connection is faced on some difficulties like voltage balance, need of more caution for the higher output voltage, cell balancing, and the mechanical stack assembly problems for arrangement.

4. Basic Operation of BOP in the PEMFC System

4.1 Fuel Storage Unit and Reformer

The function of the reformer is to convert the raw primary fuel, usually LNG, to a hydrogen-rich fuel gas that is required by the fuel cell stack, and to supply this hydrogen-rich gas to the stack. If the operation temperature of the reform process is lower, the requirement of the fuel reform process is severe. The fuel fed to a PEMFC must be CO free. Also, PEMFC can directly utilize some kind of hydrocarbons, such as propane, although their performance is poor. In case of gas such as LNG, a sulphur compound is used as an odorant by the gas utility company for user safety. However, the fuel processor catalysts are usually intolerant to sulphur, it is known that only 1 ppb is enough to permanently poison the PEM anode catalysts [1]. There are some kinds of methods for the reformer type, such as steam reforming, dry reforming, direct internal reforming, indirect internal reforming, and partial oxidation.

On the other hand, it is more convenient not to extract hydrogen from fossil gas, but rather just to store the hydrogen as hydrogen. Usually mobile applications, such as vehicles, locomotives, and portable applications use this type of fuel storage unit. But, the hydrogen is very high in energy and its density is very low, so to store a large mass of hydrogen in a small area, it needs very high pressure. In addition, hydrogen is a very volatile and flammable gas. Therefore, if the fuel cell system gets hydrogen from a storage unit, the safety of the whole fuel cell system may be compromised, and full consideration must be given.

There are several kinds of methods for hydrogen storage. The first is the storage of hydrogen as a compressed gas, which is very simple with infinite storage time. This method is widely used especially in fuel cell hybrid vehicles. The second is the storage of hydrogen as a liquid (LH_2). This is also widely used in vehicles with LH_2 gas tanks. The third is the reversible metal hybrid method. This is suitable for small portable electronic applications. Other methods involve making hydrogen-rich chemicals and are often adopted to the carriers of hydrogen.

4.2 Power Conditioning System

In distributed generation, the major purpose of the fuel cell system is the electrical generation, while in fuel cell vehicles, it is the traction drive using the electrical power of the fuel cell system. Therefore, in this kind of EBOP, the power conditioning system (PCS) plays the most important role in fuel cell applications. The fuel cell inherently has a characteristic of low output voltage and high output current compared to other power sources. Consequently, the PCS consists of a dc/dc converter, which boosts up the low fuel cell output voltage, and a dc/ac inverter that is serial-connected to the dc/dc converter, which makes the output of dc/dc converter compatible to the load such as an ac grid for embedded generation or ac machines for traction. From a design viewpoint, the dc/dc converter used in PCS has the features of high current input with low voltage and high voltage output with relatively low current. For this reason, the higher ratios of the fuel cell input voltage and the dc link voltage result in the dc/dc converter with high frequency transformer that has higher voltage ratios, galvanic isolation between the fuel cell, and dc/ac inverter output.

Fig. 4 shows the basic configuration of the PCS. In Fig. 4, PCS can be categorized by two groups, which depends on the auxiliary energy storage such as Li-ion battery or super-caps. Like stationary generation it has continuous power flow from the fuel cell to the grid or load. In this case, usually the load is constant power, and the rapid change of the load fluctuation does not often occur. In contrast, in the case of transportation units such as vehicles and locomotives, the acceleration and deceleration of speed is not rare; it depends on the traffic condition and driver's status. Therefore, an auxiliary storage unit is necessary, because the fuel cell does not respond so rapidly by nature.

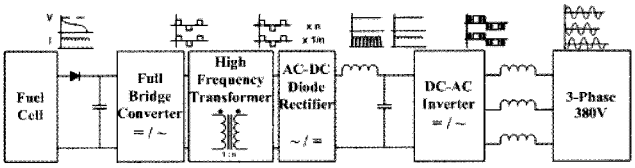

(a) PEMFC 3-phase generation system without the auxiliary storage unit

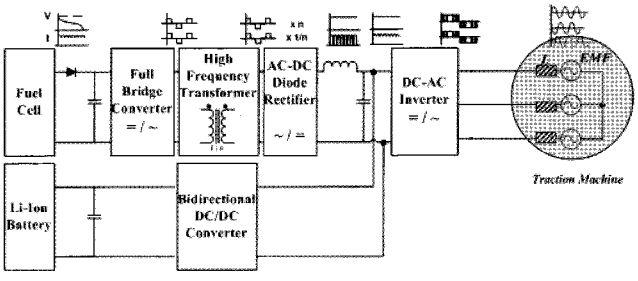

(b) PEMFC PCS with auxiliary storage unit for hybrid vehicles

Fig. 4. Block diagram of the PCS for fuel cell.

Table 2. Design parameters

PARAMETERS	VALUE	UNIT
RATED OUTPUT POWER	2	KW
INPUT VOLTAGE (PEMFC OUTPUT VOLTAGE)	22~50	V
DC LINK VOLTAGE (DC/DC OUTPUT VOLTAGE)	350	V
OUTPUT VOLTAGE (DC/AC OUTPUT VOLTAGE)	220	V
OUTPUT CURRENT (DC/AC OUTPUT CURRENT)	9.1	A
DC/DC CONVERTER SWITCHING FREQUENCY	30	KHZ
DC/AC INVERTER SWITCHING FREQUENCY	10	KHZ

The bidirectional dc/dc converter is also necessary for managing the power flow of the auxiliary storage unit, for example charging and discharging of the battery for acceleration and deceleration and controlling the SOC of the battery.

As an example, the residential single phase grid-connected PCS specification of the dc/dc converter and dc/ac inverter with PEMFC is indicated in Table II.

In the case of a voltage-fed full bridge, there is no start-up problem as experienced by the current-fed type. However, a dead time circuit is needed to avoid the shoot-through problem and a filter inductor is necessary for the output of the dc/dc converter that can smooth the output voltage ripple. The current-fed full-bridge has the input reactor in series, compared to the voltage-fed type that has the input capacitor in parallel as usual. This type of dc/dc converter has a start-up problem in that it can't start from low input voltage; therefore it needs new schemes for start-up [16]. Nevertheless, it has ZVS/ZCS characteristics by controlling the auxiliary switch. As a result the efficiency of this converter is above 92% at rated power, but the efficiency of the voltage-fed type is usually above 85% at rated power. In the dc/ac inverter, it is more usual to adopt the voltage-fed pwm inverter.

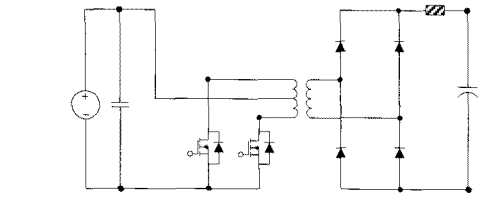

(a) Push-pull dc/dc converter

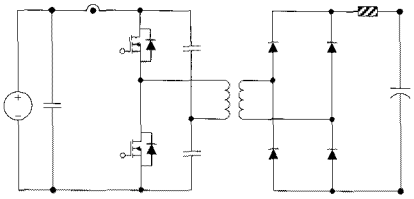

(b) voltage-fed half bridge dc/dc converter

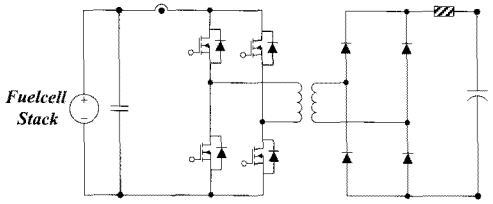

(c) voltage-fed full bridge dc/dc converter

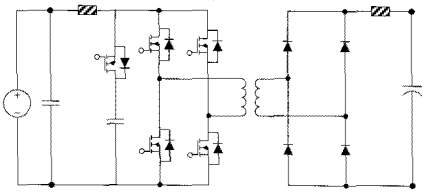

(d) current-fed half bridge dc/dc converter

Fig. 5. Various types of dc/dc converters for PEMFC

4.3. Water and Air Suppliers

In the fuel cell system, air is provided for the purpose of supplying oxygen to the cathode and cooling the fuel cell stack and system. Therefore, fans and blowers are usually used for the purpose of cooling the system, feeding the air to the fuel cell and circulating the air in the system. Simultaneously, very hot output gas is exhausted into the air by the reformer and the fuel cell stack. From this hot gas, energy can be derived by use of the turbine which makes the compressor turn. The combination of this turbine and compressor is called a turbo-compressor. The practical issue for the selection of this kind of turbo-compressor is the capacity of the compressor, because the capacity of the compressor is comparatively too big to fuel cell capacity. It is very difficult to find such a turbo-compressor less than that of a 50kW fuel cell system [1], therefore the efficiency of the compressor lessens. Pumps are also used for the purpose of circulating the reactant air and hydrogen fuel in the PEMFC. They must have the characteristics of low cost, noiselessness, reliability, low power consumption, and small volume. Above all, most of these equipments mentioned in this section are almost commercialized for other applications; therefore it is convenient not to develop these equipments, but rather just to take these parts.

5. Design of Converter and Inverter for the PEMFC System

For the convenience of PCS controller design, the conventional voltage-fed full bridge is adopted for the dc/dc converter, and a voltage-fed pwm dc/ac inverter is adopted for designing the grid-connected inverter in this paper. In designing the parallel system, the PEMFC, dc/dc converter, and dc/ac inverter is used as a module block. Consequently, the fuel cell input module consists of two PEMFCs, the two dc/dc modules consist of two voltage-fed full-bridge converters, the dc/ac module consists of a

voltage-fed pwm inverter, and the filter module consists of passive inductor and capacitor as shown in Fig. 6. If there is a problem with any module, it is easy to replace the module with a new one and reconnect it to the system.

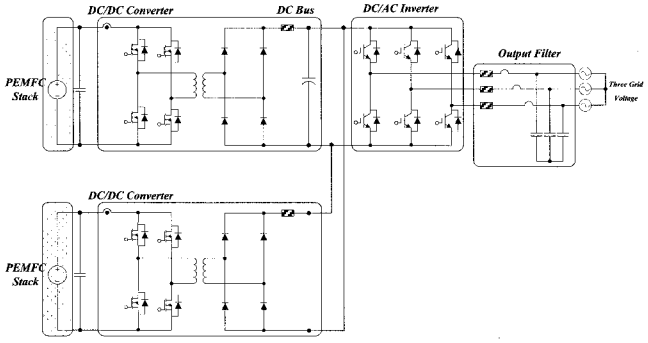

Fig. 6. Design of parallel distributed generation system using PEMFC

5.1 Design Analysis of Voltage-fed Full Bridge dc/dc Converter

To use the dc/dc converter in Fig. 5 (c) that converts the low fuel cell output voltage to the high dc link voltage, Table III shows the design parameters of the full bridge dc/dc converter.

During the half cycle of the switching period, the average inductor voltage of the converter output is equal to zero, from this inductance voltage it is defined as given in Equation (13)

$$\left(V_{in}\cdot\frac{1}{n}-\frac{V_{out}}{2}\right)\cdot\frac{DT_S}{2}=\frac{V_{out}}{2}\cdot\frac{(1-D)T_S}{2} \tag{13}$$

where, D is duty ratio, and T_s is switching time (= $1/f_s$).

Table 3. Design parameters of full bridge converter

PARAMETERS	VALUE	UNIT
RATED OUTPUT POWER	1.2	KW
INPUT VOLTAGE (PEMFC OUTPUT VOLTAGE, V_{IN})	22~50	V
DC/DC CONVERTER SWITCHING FREQUENCY (F_S)	30	KHZ
DC LINK VOLTAGE (DC/DC OUTPUT VOLTAGE, V_{OUT})	350	V
OUTPUT CURRENT (DC/DC OUTPUT CURRENT)	3.5	A
DC/DC CONVERTER SWITCHING FREQUENCY	30	KHZ
TRANSFORMER TURN RATIO (N)	3 : 52	TURN
OUTPUT INDUCTANCE	800	UH
OUTPUT CAPACITOR	1680	UF

From Equation (13), the transfer function of the voltage-fed full bridge converter is derived like in Equation (14). In Equation (14), the transformer turn ratio is roughly 1:17, but it could not be used in the common transformer-less boost converter as the dc/dc converter due to its parasitic parameters.

$$\frac{V_{out}}{V_{in}}=2D\cdot\frac{1}{n} \tag{14}$$

Calculating the power loss of this dc/dc converter, there are some assumptions.

(1) The transformer and inductor has both a copper and iron loss, copper loss is only defined by the length of the wire, and iron loss is only defined by multiplying the volume of the core [cm^3] and the loss per cubic [mW/cm^3] in the core data sheet.
(2) There are two kinds of losses defined by the switching device: the switching loss and the conduction loss. Switching loss is just calculated by multiplying of the idealized current and the voltage with the sum of switch time that is turn-on time, turn-off time, rise time, and delay time. Conduction loss is calculated by multiplying conduction current and the drain source resistance.
(3) The output characteristics of the MOSFET body diodes and the rectifier diodes are modeled by the threshold voltage V_f and the differential resistance r_f for the calculation of the conduction loss of the diode. The switching loss is calculated by the reverse recovery charge Q_{rr} [10].

Transformer and inductor copper loss is:

$$P_{cp}=n_1\cdot R_{eq1}\cdot i_1^2+n_2\cdot R_{eq2}\cdot i_2^2 \tag{15}$$

where, n_1 is the primary turns, n_2 is the secondary turns, R_{eq1} is the equivalent resistance of the primary turns, and R_{eq2} is that of the secondary turns. If there is a skin effect in the transformer, the copper loss will be 2 ~ 3 times more than calculated.

Transformer and inductor iron loss is:

$$P_{iron}=Volume_{core}\cdot Loss_{core} \tag{16}$$

A MOSFET's switching loss is:

$$P_{switching}=\frac{1}{2}\cdot V_{in}\cdot I_1\cdot(t_{on}+t_r+t_{off}+t_d)\cdot f_s \tag{17}$$

Where turn-on time is t_{on}, rise-time is t_r, turn-off time is t_{off}, and delay time is t_d.

A MOSFET's conduction loss is:

$$P_{conduction}=R_{ds,on}\cdot D\cdot i_{1,on}^2 \tag{18}$$

To reduce the conduction loss and improve PCS efficiency, low on-resistance of the power device and another switching method that reduces the switching loss such as ZCS or ZVS is a very significant to the dc/dc

converter.

A rectifier diode's switching loss is:

$$P_{switching,rect} = \frac{Q_{rr} \cdot V_{in} \cdot n}{2T_s} \quad (19)$$

A rectifier diode's conduction loss is:

$$P_{conduction,rect} = \frac{V_f \cdot I_2}{4} + \frac{r_f \cdot I_2^2}{8} + \frac{r_f}{T_s} \cdot \frac{(1-D)T_s}{2T_s} \quad (20)$$

5.2 Design Analysis of Voltage-fed pwm dc/ac Inverter

To design a single phase pwm dc/ac inverter that converts the high dc link output voltage to the single phase 220V/60Hz grid-connected ac voltage, Fig. 7 shows the schematic diagram of a dc/ac full-bridge voltage-fed pwm inverter. The inverter tracks the grid frequency and voltage. As a result it is controlled as unity power factor and the constant output power is 2kW. In this grid-connected type inverter, the inverter is connected parallel to the load with the grid input, therefore the peak power of the load is delivered from the grid input. Due to these characteristics the auxiliary storage unit is usually unnecessary, but it is necessary to locomotives, vehicles, and stand-alone type inverters. To calculate the power loss of this type of inverter, the switching loss is the same as Equation (17). However, in conduction loss, it is the same as Equation (21). Table IV shows the design parameters of the dc/ac inverter.

An IGBT's conduction loss is calculated like:

$$P_{conduction} = V_{sat} \cdot i_{2,rms} \quad (21)$$

In general, the efficiency of the dc/ac inverter is typically 95~97%. Consequently, it rarely changes its topologies and the unipolar pwm method which can reduce the output filter size and switching loss. Also, in grid-connected PCS, the total harmonic distortion factor (THD) is regulated to below 5% and each harmonic term of the output current is regulated to below 3%. In addition, the anti-islanding algorithm to shutdown PCS operation when

Table 4. Design parameters of pwm inverter

PARAMETERS	VALUE	UNIT
RATED OUTPUT POWER	2	KW
INPUT VOLTAGE (DC INPUT VOLTAGE, V_{IN})	350	V
AC INVERTER SWITCHING FREQUENCY (F_S)	10	KHZ
OUTPUT CURRENT (AC OUTPUT CURRENT)	9.1	A
OUTPUT VOLTAGE (AC OUTPUT VOLTAGE)	220	V
OUTPUT INDUCTANCE	3	MH
OUTPUT CAPACITOR	5	UF

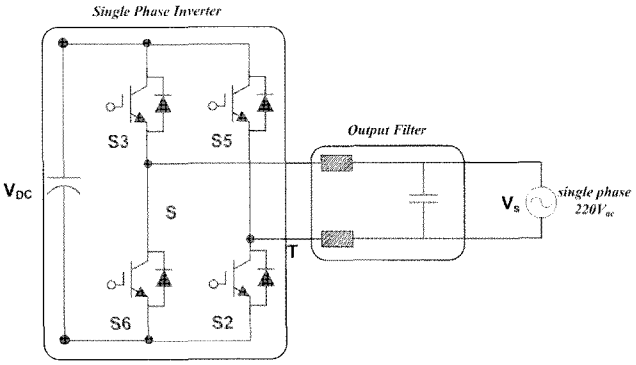

Fig. 7. Voltage-fed pwm dc/ac inverter for grid-connected PCS

the power failure occurs is necessary within 0.5sec after the power failure happens. In the case of the three-phase system, one more switching arm is added, as shown in Fig. 7, and also one more output filter inductor and output filter capacitor is needed for the three-phase grid. In Fig. 7, the single phase grid-connected inverter is shown, and the grid voltage is 220V, 60Hz in general.

5.3 Analysis of Parallel Imbalance in dc/dc Converter

For the parallel operation of two independent sources, two PEMFC modules and two dc/dc converters are used in this paper. There are two ways of parallel operation, one is dc/ac inverter parallel operation, and the other is dc/dc converter parallel operation. Performing parallel operation by dc/ac inverter provides a satisfactory result from the perspective of the simple control method. From the viewpoint of unity power factor control, there is inherent PLL loop in grid-connected PCS, therefore there should be PLL in the dc/ac PCS inverter. If the dc/ac inverter is parallel operated, it is exactly the same as two PCS operation, in which the function of sharing load is performed. In this way it is the same to operate two independent PCSs, consequently the space, cost, and the complexity are larger. For this reason, the parallel operation of the two PEMFC modules is performed in the dc/dc converter unit. However, if two independent input sources are used, the current imbalance problem is induced by the impedance difference of the two dc/dc converter module. Fig. 8 represents the equivalent model of two full bridge dc/dc converters in parallel with two PEMFC inputs. Since the current through the load is shown in Equations (22) and (23), if Z_A is not equal to Z_B, the output voltage and current sharing control is not properly performed. Therefore, the parallel operation of the dc/dc converter needs to control the current and load sharing.

$$I_A = \frac{V_{FC1} - I_B Z_L}{Z_A + Z_L} \quad (22)$$

$$I_B = \frac{V_{FC2} - I_A Z_L}{Z_B + Z_L} \quad (23)$$

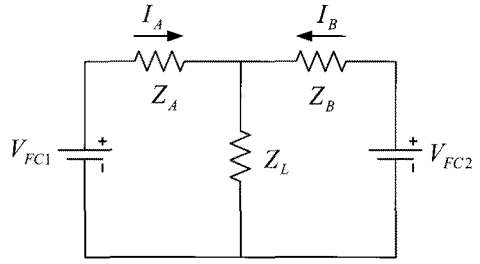

Fig. 8. Equivalent model of 2-paralleled dc-dc converter.

5.4 Design of Parallel Operation in PEMFC Generation System

The usually adopted average current sharing control algorithm is depicted in Fig. 9. In order to get a current reference, the output dc link voltage (V_o) of the dc-dc converter is measured. The measured voltage and reference voltage (V_{ref}) of the dc link are compared and its result becomes voltage error. This error signal becomes the current reference (I_{ref}) of the system through the voltage PI controller. Usually, in the case of two converter parallel operation, one half of I_{ref} is transmitted on each current controller of both converters. In the case of the parallel operation of N converters, the current reference of each converter is calculated by $1/N$ times. But, this method results in a slow and smooth voltage response like under-damping and a short time imbalance of the dc/dc converter because when the converter is increased by N, the whole current and voltage response that is shared by the N dc/dc converter is not the same as that of the one converter from which the reference is not divided. Therefore, in this paper, the gain adjustor block is suggested as is shown in Fig. 10. This is the attenuation block of the gain by the number of dc/dc converters. It could be a gain table by the number of N or the outputs of state equations of N dc/dc converters. These current references are compared with saw-tooth signal in which pulse width modulation (pwm) signal is generated by the analog controller. This pwm signal regulates the voltage output of the converter. Therefore, current distribution of the voltage PI controller output can be uniformly performed by the gain adjustor block without 1/N times of current reference. The Gain adjustment controller could increase the gain of the N voltage controller up to the value exactly identical to the gain that only one voltage controller has done.

In this voltage and current control loop, the voltage and current are controlled by digital and analog controller, respectively. The response of the current controller should be set at high cut-off frequency through the analog controller. Simultaneously, in the case of the voltage

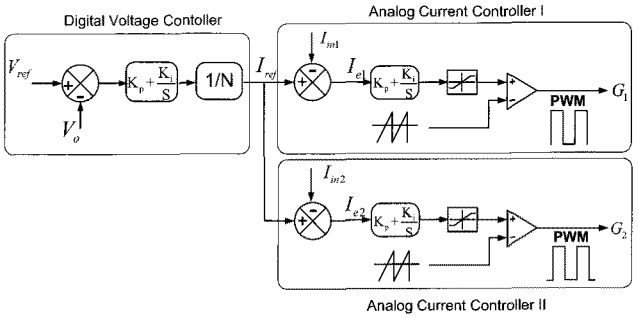

Fig. 9. Current sharing method of paralleled dc/dc converter by 1/N reference.

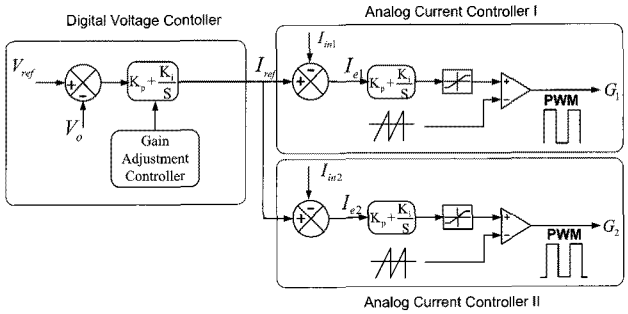

Fig. 10. Current sharing method of paralleled dc/dc converter by gain adjustor.

controller, the cut-off frequency could be set lower than the current controller. The sampling time by the digital controller does not affect the control performance of the analog controller. The implementation of these controller configurations is explained below.

Fig. 11 indicates the voltage control scheme with use of the average current control of PEMFC stack output current. There is only one dc link capacitor block in the implements of this paper. The output voltage of each dc/dc converter is sunk in only one dc link capacitor block. The inner current loop has a fast response time compared to the outer voltage loop and the cut-off frequency of the inner loop is at least three times higher than that of the outer loop. Through this compensation loop, each of the inner current loops performs the current sharing for the two dc/dc converter

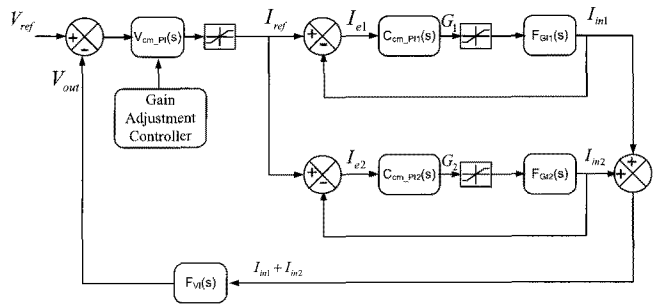

Fig. 11. Control scheme for parallel PCS operation of distributed generation.

load. The closed loop state function is obtained as Equations (24) and (25).

$$\frac{V_{out}}{V_{ref}} = \frac{F_{gi}(s) \cdot F_{vi}(s) \cdot V_{cm\_pi}(s)}{1 + F_{gi}(s) \cdot F_{vi}(s) \cdot V_{cm\_pi}(s)} \tag{24}$$

$$F_i(s) = F_{i1}(s) + F_i2(s) = \frac{C_{cm\_pi1}(s) \cdot F_{gi1}(s)}{1 + C_{cm\_pi1}(s) \cdot F_{gi1}(s)} + \frac{C_{cm\_pi2}(s) \cdot F_{gi2}(s)}{1 + C_{cm\_pi2}(s) \cdot F_{gi2}(s)} \tag{25}$$

Therefore in parallel operation, any one digital controller of the two PCS is set in master mode, and automatically the other one is set in slave mode. In master mode, PCS senses dc link voltage, compares dc link voltage to the reference, and makes errors for input of the digital PI controller in the master controller. The output of the voltage PI controller is the current reference for the analog controller of both master and slave PCS, and the digital controller converts this value to analog by use of the DA converter. Consequently, the analog current reference, which is the DA converter output, is the input for the analog controller of both PCS, usually using a commercial pwm controller, like TL494, UC3845, etc…

6. Implementation of Parallel Generation System Using PEMFC

As indicated in Fig. 12 (a) ~ (c), the implementation of the distributed generation system with two dc/dc converters, a dc/ac single phase grid-connected inverter, and two PEMFCs is performed in a laboratory. Building up the 2kW parallel operated generation system in a laboratory consists of two PEMFC modules with a hydrogen storage unit (shown in Fig. 12(a), an 1.2kW Ballad Nexa PEMFC system), a single phase grid-connected master PCS (as shown in Fig. 12(b)) and a slave mode parallel operated dc/dc converter (as shown in Fig. 12(c)) for parallel operation of the distributed generation system. The whole configuration is shown in Fig. 12 (c), it can only be set up with a 2kW standard single phase grid-connected dc/ac inverter (shown in Fig. 12 (b)) and two dc/dc converters as master and slave mode converters. The PCS has an analog and digital controller, already explained above in Section V.

The PCS consists of a dc/dc converter and dc/ac inverter. A 1.2kw interleaved voltage-fed full bridge dc/dc converter and dc/ac inverter control parts are composed of the digital DSP controller of Freescale's 56F803 and analog controller of TI's TL494. DSP 56F803 is implemented to realize the digital voltage controller with 10kHz, and a dc/ac inverter that has switching frequency of 10kHz for ac voltage grid connection. TL494, the analog pwm controller, is implemented for the analog current controller with 30kHz

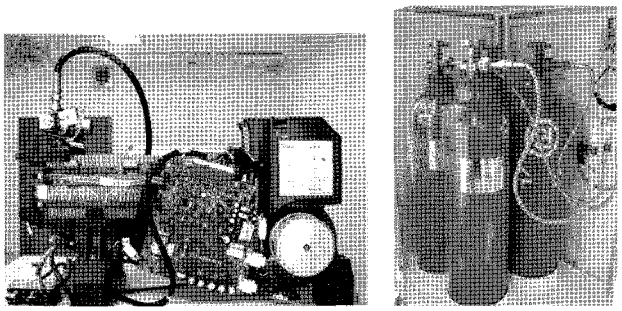

(a) an 1.2kw Ballad Nexa PEMFC module with storage unit

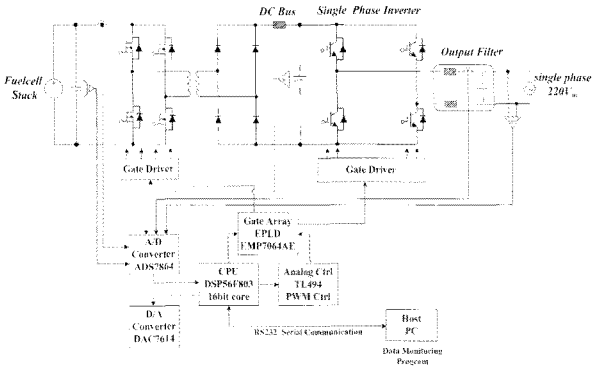

(b) Single phase PCS configuration with digital/analog controller

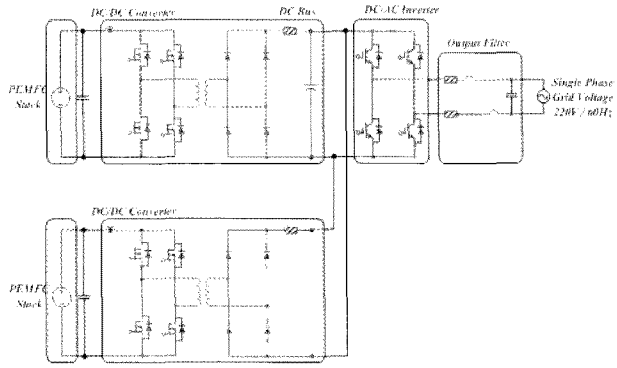

(c) Experimental diagram of parallel operation system

Fig. 12. Implementation of the parallel operation system using PEMFC

switching frequency for current controller of the dc/dc converter. In the dc/dc converter, TL494 is enabled by the DSP controller and the soft-start function, which causes the dc link voltage to build up slowly when the converter is enabled. If there is a fault in the PCS hardware (such as high input/output current, high input/output voltage, low input/output voltage, power line loss, over-temperature…) or in converter or inverter hardware, the DSP controller detects this situation, stops the entire generation system and alerts the host controller (like PC) by RS-232 serial communication. The two PCS configurations and the control B/D are shown in Fig. 13 (a). Two PCSs act as a master mode PCS (dc/dc converter and dc/ac inverter is

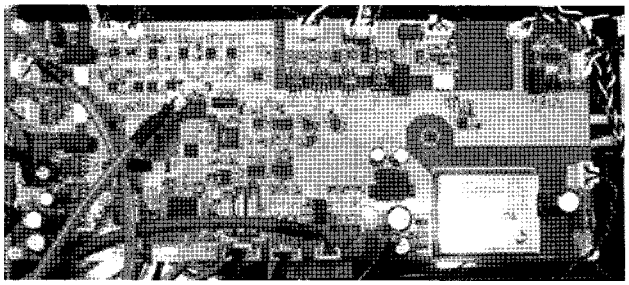

(a) Control board with 56F803 & TL494 controller, gate ICs, and sensing units.

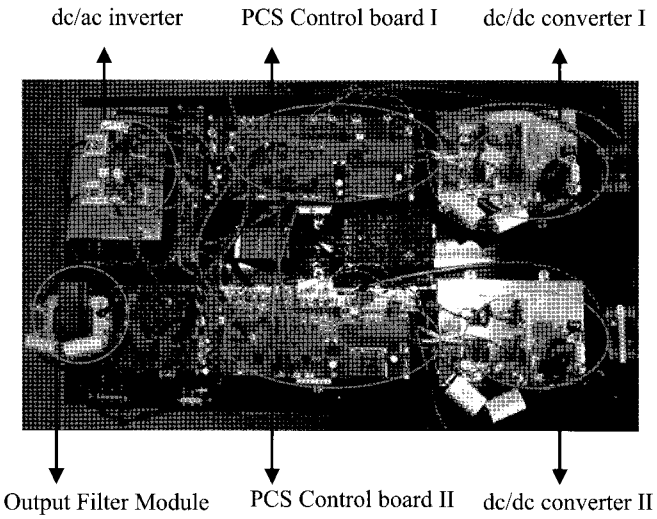

(b) PCS of parallel operation system

Fig. 13. Implementation of the parallel generation system using PEMFC

implemented) and slave mode PCS (only dc/dc converter part is implemented). Also in a PCS control board, the gate ICs of the converter and inverter using boot-strap topology and current and voltage sensing ICs are on the same board. In the parallel distributed generation system, there is only one dc/ac inverter unit which is connected to the master controller of the DSP 56F803.

Generally, it is easier to increase the capacity of the dc/ac inverter than that of dc/dc converter due to low input current characteristics of dc/ac inverter compared to relative high input current of the dc/dc inverter. Also, in Fig. 13 (b), the parallel operated PCS is shown with only one dc/ac inverter.

7. Influence of Parasitic Parameters Due to Parallel Operation of PEMFC

With parallel operation of the dc/dc converter, parasitic impedance is induced by the relative long distance of input (leakage inductance) and the transformer coupling (leakage capacitance). Generally designing the dc/dc converter, the implementation of the circuit is tight and slim for reducing parasitic impedance, especially for leakage inductance and coupling capacitance. But, for paralleling the dc/dc converter, the line distance is increased and the circuit area is increased by high input current and the size of the power device is also increased by the highly required power rate. By this reason the influence of the parasitic parameter is not ignored.

Fig. 14 (a) gives the diagram of the dc/dc converter including this parasitic parameter. Generally speaking, the influence of input leakage inductance is shown as the voltage spike of the input power device, MOSFET, since input current or input voltage is larger. To reduce this spike, usually the film capacitor is added on the circuit as the over-voltage snubber. However, addition of the over-voltage snubber also induces voltage oscillation with input leakage inductance, because inductance of the parallel circuit is not a small value any more, despite using the bus-plate as shown in Fig. 13 (b) and even if the bus-bar as the input MOSFET connection is not used. As a result, the secondary side voltage of the transformer becomes large enough to break down the secondary side bridge diode, for which the voltage rating of the secondary diode is 1200V. If this snubber capacitor is reduced, the voltage spike of MOSFET is increased again, enough to break down the MOSFET. Therefore, there is a trade-off for deciding over voltage snubber capacitor value by the spike magnitude of both power devices. Also, the parasitic coupling capacitance of the transformer affects the voltage oscillation across the secondary side bridge diode and this is another source of the voltage spike that induces voltage breakdown of secondary bridge diodes or ringing voltage that reduces efficiency of the dc/dc converter. In Fig. 14 (b) and (c), these side effects are simulated by PSIM with a 10uF over voltage snubber. Table V presents the parasitic parameter and the power device rating that is used in this simulation and the experiments.

To solve this problem, a snubber circuit, which is introduced in [12], is added on the secondary side of the transformer. It is a lossless snubber, called CDD snubber, therefore it does not affect the efficiency of the dc/dc converter. Fig. 14 (d) shows the schematic diagram of this

Table 5. Design Parameters of parasitic componets and power devices

PARAMETERS	VALUE	UNIT
INPUT VOLTAGE	50	V
INPUT SWITCHING DEVICE VOLTAGE RATING	200	V
SECONDARY BRIDGE DIODE VOLTAGE RATING	1200	V
OUTPUT FILER INDUCTANCE	800	UH
OUTPUT FILER CAPACITANCE	300	UF
INPUT LEAKAGE INDUCTANCE	500	NH
TRANSFORMER COUPLING CAPACITOR	1	NF

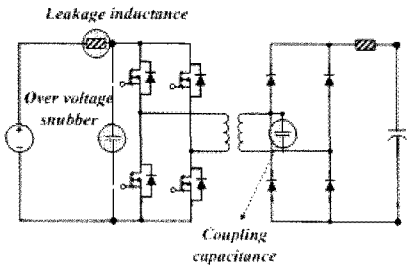

(a) Simulation scheme considering parasitic parameters with snubber

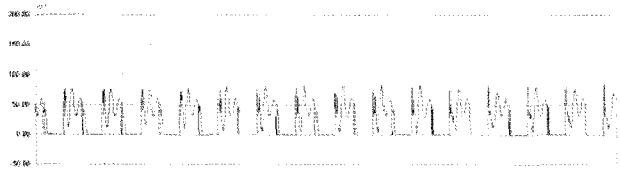

(b) Voltage spike of primary side MOSFET with over-voltage snubber

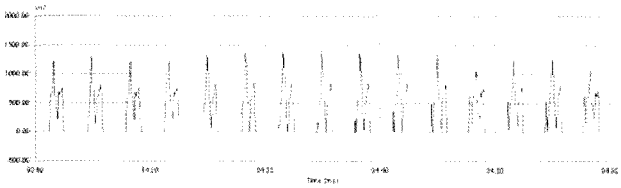

(c) Voltage spike of secondary side diode with the influence of primary side over-voltage snubber

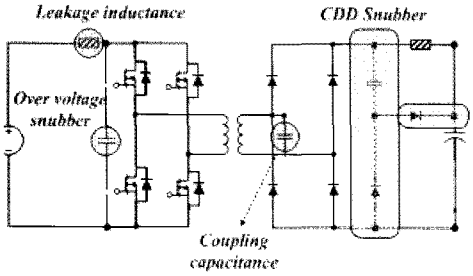

(d) Simulation scheme considering parasitic parameters with CCD snubber

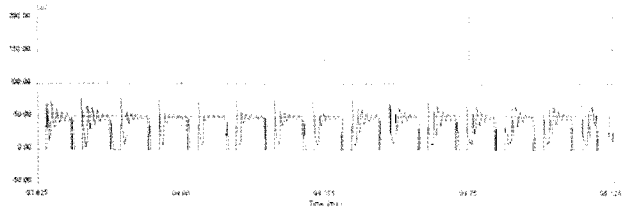

(e) Voltage spike of primary side MOSFET with over-voltage snubber & CCD snubber

(f) Voltage spike of secondary side diode with the influence of primary side over-voltage snubber & CCD snubber

Fig. 14. Simulation result considering parasitic parameter with CCD snubber

CDD snubber, and Fig. 14 (e) and (f) present the simulation result of the circuit shown in Fig 14 (d).

Compared to (b) and (e) the voltage spike of primary side MOSFET is little increased but the secondary diode voltage in Fig. 14 (c) and (f) is reduced by 400 ~ 500V. Therefore, it is enough to use the diode voltage rating of under 1200V, not 1700V, because the 1200V rating is more common than 1700V. For the use of input power device voltage rating, 200V is sufficient due to fact that the input maximum voltage range is 50V. And the bus plate is also used for reducing the leakage inductance. Compared to when bus bar structure is used as input MOSFET connection instead of bus plate, it reduces the secondary voltage spike about 50 ~ 100V.

8. Experimental Result of Parallel Generation of PEMFC

In Fig. 15 (a) ~ (d), the experimental results of the parallel distribution generation system are shown, whose schematic diagram is the same as Fig. 12 (c). In Fig. 15 (a), it shows that the input voltage and current of the master and slave dc/dc converter is identical to each other, therefore the load sharing of two PEMFCs is properly performed by the accordance with the control design of Fig. 10 and Fig. 11. And the CDD snubber circuit that is already explained in Section VII is added in the PCS, therefore the switching voltage spike and secondary diode spike is also reduced as indicated in Fig. 15 (b) ~ (c) by acceptable range. As a result, the output grid voltage and gird current have the unity power factor and the output power whose value is 2kw by the two PEMFC generation systems properly performed as shown in Fig. 15 (d).

9. Conclusions

In this paper, the feasibility design of parallel operation for distributed generation using PEMFC systems is introduced and explained in order to increase the PEMFC capacity. Considering the parallel operation of PCS and two PEMFC systems, the influence of parasitic impedance is increased by growing size, capacity, and power rating of the distributed generation system. In N-parallel operation control design, the gain adjustment method has the simple and fast response to achieve parallel operation and load sharing compared to the method that has the same reference divided by N. Also, all proposed design methods for the parallel operation are accomplished by the two PEMFC systems, two dc/dc converters, and a dc/ac inverter in the laboratory. The simulation of parasitic parameter influence and the PEMFC parallel operation

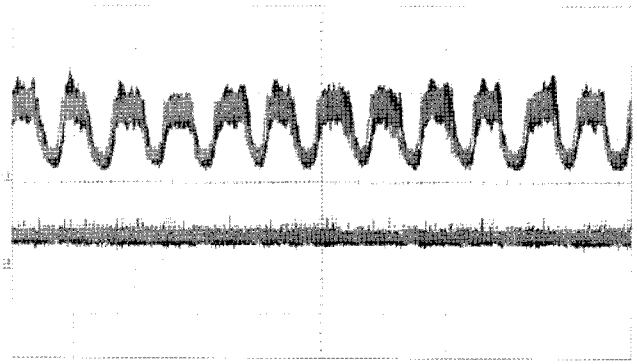

(a) Input current (20A/div) / Input voltage (50V/div) of master and slave dc/dc converters in parallel distributed generation

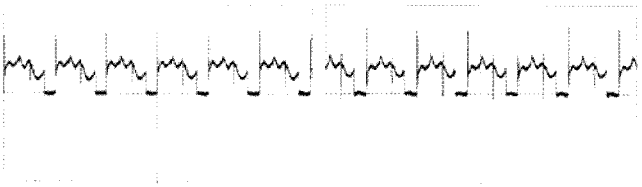

(b) MOSFET switching voltage (25V/div) of master and slave dc/dc converters in parallel distributed generation

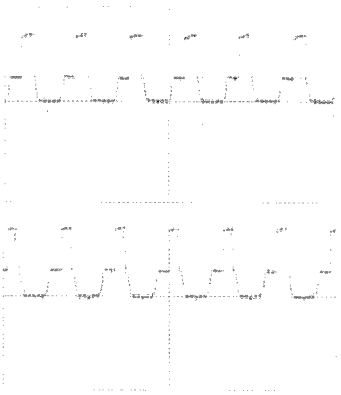

(c) Secondary diode voltage (200V/div) of master and slave dc/dc converters in parallel distributed generation

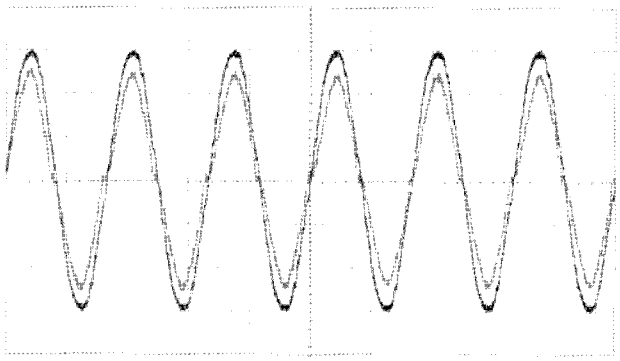

(d) Output grid voltage (100V/div) and output grid current (5A/div) of dc/ac inverter in parallel distributed generation

Fig. 15. Experimental results in parallel distributed generation

experimental results are also provided. With this proposed design method, the PEMFC can have the attractive merits by expansion of its capacity. With just a simple current reference expansion method by the addition of gain adjustor, the parallel operation can be achieved and the load sharing is accomplished. Therefore, it is also expected that, by use of this proposed design method, an optimal design of parallel PEMFC system operation could be performed for various fuel cell applications such as vehicles, locomotives, and IPGs.

References

[1] J. Larminie and A. Diks, "Fuel cell system explained, 2nd ed," JOHN WILEY & SONS, LTD.

[2] R. K. Ahluwalia and X. Wang, "Fuel cell systems for transportation: Status and trends," *Journal of Power Source*, vol. 177, pp. 167-176, 2008.

[3] L. A. Riascos, M. G. Simoes, and P. E. Miyagi, "On-line fault diagnostic system for proton exchange membrane fuel cells," *Journal of Power Source*, vol. 175, pp. 419-429, 2008.

[4] J. Stumper and C. Stone, "Recent advances in fuel cell technology at Ballard," *Journal of Power Source*, vol. 176, pp. 468-476, 2008.

[5] G. Y. Choe, J. S. Kim, H. S. Kang, B. K. Lee, and W. Y. Lee, "PEMFC modeling for high efficiency fuel cell BOP," *ICEMS*, 2007.

[6] D. K. Choi, B. K. Lee, S. W. Choi, C. Y. Won, and D. W. Yoo, "A novel power conversion circuit for cost-effective battery-fuel cell hybrid systems," *Journal of Power Source*, vol. 152, pp. 245-255, 2005.

[7] T. W. Lee, J. Hur, B. K. Lee, and C. Y. Won, "Design of a fuel cell generation system using a PEMFC simulator," *Electric Power Systems Research*, vol. 77, pp. 1257-1264, 2007.

[8] H. S. Chu, F. Tsau, Y. Y. Yan, K. L. Hsueh, and F. L. Chen, "The development of a small PEMFC combined heat and power system," *Journal of Power Source*, vol. 176, pp. 499-514, 2008.

[9] A. R. Miller, K. S. Hess, D. L. Barnes, and T. L. Erickson, "System design of a large fuel cell hybrid locomotive," *Journal of Power Source*, vol. 176, pp. 499-514, 2008.

[10] M. Mohr and F. W. Fuchs, "Voltage fed current fed full bridge converter for the use in three phase grid connected fuel cell systems," *IPEMC*, vol. 1, 2006, pp.1-7.

[11] X. Kong and A. M. Khambadkone, "Analysis and implementation of a high efficiency, interleaved current-fed full bridge converter for fuel cell system," *PEDS*, vol. 1, 2005, pp. 474-479.

[12] J. G. Cho, J. W. Baek, C. Y. Jeong, G. H. Rim, "Novel zero-voltage and zero-current-switching full-bridge pwm converter using a simple auxiliary circuit," *IEEE Trans. on IA*, vol. 35, no. 1, pp. 15–20, Jan/Feb. 1999.

[13] M. Ilic and D. Maksimovic, "Phase-shifted full bridge dc-dc converter with energy recovery clamp and reduced circulating current," *APEC*, 2007, pp. 969-975.

[14] X. Jiang, X. Wen, and H. Xu, "Study on isolated boost full bridge converter in FCEV," *IPEC*, vol.2, 2005, pp. 827-830.

[15] Ballard Nexa® Power module user's manual.

[16] L. Zhu, K. Wang, F.C. Lee, and J. Lai, "New start-up schemes for isolated full-bridge boost converters," *IEEE Trans. on PE*, vol. 18, no. 4, pp. 946–951, 2003.

Hyun-Soo Kang (S'07)
He received his B.S. and M.S. degrees from Hanyang University, Seoul, Korea, in 1994 and 1996 in Electrical Engineering. From 1996 to 1999, he was an Associate Research Engineer at Power Electronics Lab., LGIS R&D Center, Anyang, Korea. In the year 2000, he joined ADT Co., Ltd., where he is now a Principal Engineer in the R&D Center. Also from 2006, he has been enrolled in a Ph.D. course at Sungkyunkwan University, Suwon, Korea His research interests include sensorless drives for IM and PM motor drives, power conditioning systems for renewable energy sources, and power electronics.

Gyu-Yeong Choe (S'08)
He received his M.S. degree from Sungkyunkwan University, Suwon, Korea, in 2008. Since that time he has been enrolled in a Ph.D. course at Sungkyunkwan University, Suwon, Korea. His research interests include fuel cell modeling, interleaved dc/dc converters, and power conditioning systems for PEMFC.

Byoung-Kuk Lee (S'97, M'02, SM'04)

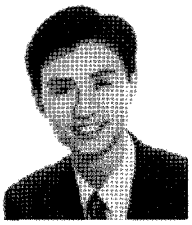

He received his B.S. and M.S. degrees from Hanyang University, Seoul, Korea, in 1994 and 1996, respectively, and his Ph.D. degree from Texas A&M University, College Station, TX, in 2001, all in Electrical Engineering. From 2003 to 2005, he was a Senior Researcher at Power Electronics Group, Korea Electrotechnology Research Institute (KERI), Changwon, Korea. From 2006, Dr. Lee joined the School of Information and Communication Engineering, Sungkyunkwan University, Suwon, Korea, as an Assistant Professor. His research interests include sensorless drives for high speed PM motor drives, power conditioning systems for fuel cells, modeling and simulation, and power electronics. Prof. Lee is a recipient of the Outstanding Scientists of the 21st Century award from IBC and is listed on the 2008 Ed. of Who's Who in America. Prof. Lee is an Associate Editor at the IEEE Transactions on Industrial Electronics.

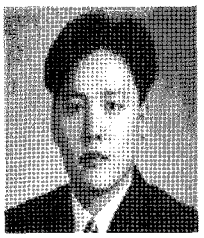

Jin Hur (S'93–M'98–SM'03)
He received his Ph.D. degree in Electric Engineering from Hanyang University, Seoul, Korea, in 1999, for research on the design and analysis of electric machines. From 1999 to 2000, he was a Postdoctoral Research Associate at the Department of Electric Engineering, Texas A&M University, College Station. From 2000 to 2001, he was a Research Professor of Electrical Engineering for BK21 projects, Hanyang University. From 2003 to 2005, he was a Director at the Intelligent Mechatronics Research Center, Korea Electronics Technology Institute, Puchon, Korea, From 2008, Dr. Hur joined the School of Electric Engineering, University of Ulsan, Ulsan, Korea, as an Assistant Professor. He is the author of over 120 publications in electric machine design, analysis and control, and power electronics. He is the holder of ten granted and pending Korea patents, one patent pending in the US and one in Japan. His current research interests include high-performance electrical machines, modeling, drives, new concept actuators for special purposes, and power conditioning systems for fuel cells. Prof. Hur is an Associate Editor in the IEEE Transactions on Power Electronics